Journal of Sound and Vibration 331 (2012) 638–650

Contents lists available at SciVerse ScienceDirect

Journal of Sound and Vibration

journal homepage: www.elsevier.com/locate/jsvi

Vibration and sound of an elastic wing actuated at its leading edge

A. Manela *

Faculty of Aerospace Engineering, Technion—Israel Institute of Technology, Haifa 32000 , Israel

ARTICLE INFO

Article history:
Received 14 April 2011
Received in revised form
13 August 2011
Accepted 27 September 2011
Handling Editor: J. Astley
Available online 13 October 2011

ABSTRACT

The motion and sound of a thin elastic plate, subject to uniform low-Mach flow and actuated at its leading edge, is studied. The linearized response to arbitrary small-amplitude translation and rotation is analyzed using Fourier decomposition of the forcing signal. Both periodic (sinusoidal) and non-periodic (“step-jump”) actuations are investigated. When the frequency spectrum of the forcing signal contains an eigen-frequency Ω_{res} of the unforced system, a resonance motion is excited and the plate oscillates at the corresponding eigenmode. The dynamical description is applied to formulate the acoustic problem, where the sources of sound include the plate velocity and fluid vorticity. Acoustic radiation of a dipole type is calculated and discussed in the limit where the plate is acoustically compact. In the case of sinusoidal excitation, plate elasticity has two opposite effects on sound radiation, depending on the forcing frequency: at frequencies close to Ω_{res}, the near-resonance motion results in the generation of high sound levels; however, at frequencies far from Ω_{res}, plate elasticity reduces the amplitude of plate deflection (compared to that of a rigid plate), leading to noise reduction. In the case of non-periodic actuation, the plate-fluid system amplifies those frequencies that are closest to Ω_{res}, which, in turn, dominate the acoustic signature. The results identify the trailing edge noise as the main source of sound, dominating the sound generated by direct plate motion. We suggest the present theory as a preliminary tool for examining the acoustic signature of flapping flight, common in insects and flapping micro-air-vehicles.

1. Introduction

The dynamics and sound of a thin elastic filament subject to fluid loading is a well known problem in fluid–structure interactions and has been studied extensively over the years [1–4]. Recently, the problem has attracted growing interest owing to its relevance to engineering applications and biological phenomena. These include the phenomenon of paper flutter and its importance in amending production processes in commercial printing [5]; the role of flapping motion in improving propulsive efficiency of swimming [6]; and the potential use of flow-induced motions of flexible bodies as a source of ‘green’ energy [7–9]. The acoustic problem is relevant for the analysis of bioacoustic and industrial applications, such as palatal snoring [10,11]; the effect of an acoustic field on the aerodynamic performance of micro-air-vehicle wings [12]; and the design of flapping-based active noise control systems for the reduction of blade–vortex interaction noise [13,14]. In addition, strong coupling between structure elasticity, leading edge actuation and flow vorticity is common in insect flight, where low thickness-to-chord wing ratios enable significant active and passive flapping motions [15]. These motions result in the radiation of a wide variety of noises known as “insect songs” [16,17], which are important factors in

* Tel.: +972 48292237; fax: +972 48292030.
E-mail address: avshalom@aerodyne.technion.ac.il

0022-460X/$ - see front matter © 2011 Elsevier Ltd. All rights reserved.
doi:10.1016/j.jsv.2011.09.020

the social and sexual behavior of various insect species (e.g., [18]). Consequently, several works have studied the sound field of insect-wing configurations, both experimentally [19] and numerically [20].

A major part of the theoretical works analyzing fluid–plate interactions have focused on the motion of an elastic filament subject to *uniform* axial flow. The dynamical problem in this case is governed by a balance between plate inertia, elasticity and fluid loading. Linearized stability analyzes have been carried out to determine the critical conditions for the onset of structure motion [21–24], while other works have considered the non-linear motion evolving at super-critical conditions [25–27]. The *forced* motion of a thin flexible body, resulting from active boundary actuation or unsteadiness of the incoming flow, has been studied in a separate set of works [28–30]. In an effort to analyze the biofluidic mechanism of small-scale flapping flight, recent interest in the forced-motion problem has focused on the particular case of periodic leading edge actuation. Godoy-Diana et al. [31] studied the vortex streets produced by a rigid pitching foil in a hydrodynamic tunnel. The effect of airfoil elasticity was then introduced and studied both experimentally [32] and numerically [33,34]. Alben [35] examined the linearized (small amplitude) motion of a pitching appendage and calculated the optimal flexibility required for maximum propulsion efficiency in the absence of wing inertia. In a later contribution [36], the large-amplitude motion was considered together with the effect of combining heaving and pitching motions. Michelin and Llewellyn Smith [37] included the effect of airfoil inertia and studied the dynamics of a heaving flexible wing. At certain actuation frequencies, a resonance motion was excited and rationalized in terms of the frequency spectrum of the unforced problem. In their conclusions section, the authors have indicated the importance of studying more realistic flapping schemes, and including pitching actuation in their model, to study the influence of relative phase differences between heaving and pitching motions on actual flapping pattern of an insect wing.

The acoustic problem, namely the calculation of sound produced by leading edge actuation of an elastic plate, has received considerably less attention. Previous works have focused on different setups and examined the scattering of sound from interaction of rigid structures with unsteady flows [38] or on sound radiation from fluid–structure interactions of flexible structures with uniform flow [24]. Other works have investigated the effects of boundary conditions and various forms of external forcing. Abrahams [39,40] studied the low-Mach acoustic scattering from a plate clamped at both edges and subject to heavy fluid loading. Crighton [41] investigated the relation between vibration and sound by applying a line force and geometrical inhomogeneities to the structure. Howe [42] considered the sound produced by the interaction of a line vortex with a spring-supported rigid plate. Recently, the combined effect of structure elasticity and incoming-flow unsteadiness on the acoustic radiation of a thin plate was analyzed for a flexible plate interacting with a line vortex [43].

The primary objective of the present work is to investigate the far-field acoustic signature of an elastic plate actuated at its leading edge. Toward this end, we extend existing studies of the dynamical problem by considering the system response to arbitrary small-amplitude leading edge actuations. We consider a linearized problem, where both leading edge translation and rotation are prescribed, and analyze the two-dimensional forced motion. The analysis is then applied to predict the far-field acoustic radiation, taking into account both structure dynamics and trailing edge noise contributions. While the present theory is not expected to capture the detailed dynamics of three-dimensional flapping-flight motion, it is aimed at examining the basic coupling between wing elasticity, leading edge excitation and sound radiation. This may supply a preliminary tool for evaluation and further study of the resulting acoustic signature.

The paper is organized as follows: the dynamical problem is formulated and analyzed in Section 2. The acoustic field is calculated in Section 3. The general scheme is then applied to study the system response to sinusoidal and "step-jump" actuations in Sections 4 and 5, respectively. A summary of our findings is outlined in Section 6.

2. Dynamical problem

Consider a thin elastic plate of thickness λ, length L, span l, mass per unit area $\rho_s\lambda$ and bending rigidity EI [with E the Young's modulus and $I=\lambda^3/12(1-\nu^2)$ the moment of inertia per unit span; ν is the Poisson ratio of the material]. The plate is subject to low-Mach high-Reynolds number uniform flow of speed U in the x_1-direction (parallel to the unperturbed plate chord) and is free to vibrate at its trailing edge (Fig. 1). The plate is actuated at its leading edge ($x_1=0$) with prescribed time-dependent displacement $L\varepsilon_h\Phi(t)$ in the x_2-direction and rotation $\varepsilon_p\Psi(t)$ about the x_3-direction. The length of the plate L is assumed much smaller than its span l such that the motion may be regarded as two-dimensional. Both ε_h and ε_p are taken small (and $\Phi(t),\Psi(t)\sim O(1)$) so that the following analysis can be based on linearized theory. We neglect any flow disturbances that may occur owing to leading edge actuation (e.g., the release of leading edge vortices). A similar assumption has been made in other works studying the response to small-amplitude heaving and pitching actuations [35–37].

The equation of motion of the plate, governing the plate deflection $\xi(x_1,t)$ in the x_2-direction, is given as a balance between plate inertia, bending stiffness and pressure force exerted by the surrounding fluid. A non-dimensional representation of the problem is obtained by scaling the place coordinate x_1 and plate deflection ξ by the plate length L; the time t by the convective time-scale L/U; and the pressure force by ρ_0U^2, where ρ_0 is the mean fluid density. Under the above conditions, the unsteady deflection $\xi(x_1,t)\ll 1$ of the plate satisfies the linearized equation

$$\mu\frac{\partial^2\xi}{\partial t^2}+\frac{\mu}{\alpha^2}\frac{\partial^4\xi}{\partial x_1^4}-\Delta P(\xi)=0, \tag{1}$$

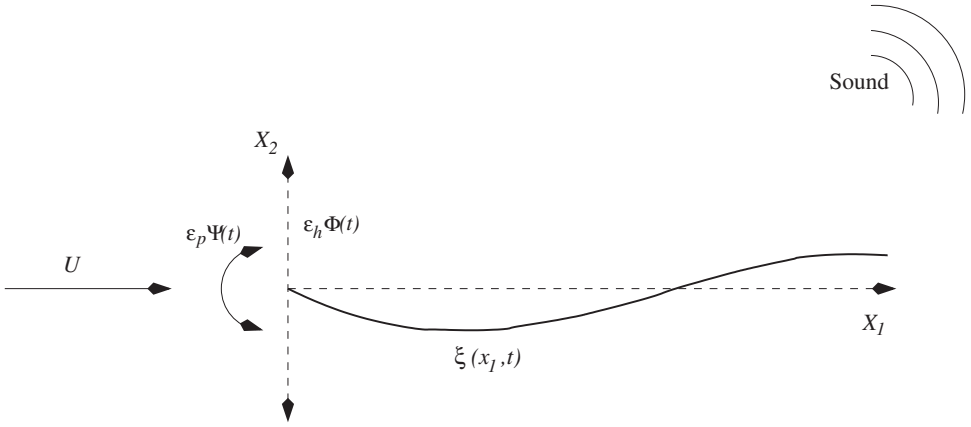

Fig. 1. Schematic of the problem. A thin elastic plate $\xi(x_1,t)$ is displaced in the x_2-direction (with $\varepsilon_h\Phi(t)$) and rotated about the x_3-direction (with $\varepsilon_p\Psi(t)$) at its leading edge, $x_1=0$. The plate is subject to uniform low-Mach stream at speed U in the x_1-direction.

where

$$\mu=\frac{\rho_s\lambda}{\rho_0 L}\quad\text{and}\quad\alpha=\frac{U}{U_b} \tag{2}$$

denote the nondimensional plate mass and wind speed, respectively, with $U_b=\sqrt{EI/\rho_s\lambda L^2}$ a characteristic bending wave speed. Also appearing in (1), is the pressure force $\Delta P(\xi)$ exerted by the fluid across the plate in the direction of increasing ξ. In what follows, we regard the plate as a flexible wing and apply linearized thin airfoil theory [44,45] to model the effect of fluid loading in the equation of motion. Explicit expression for the Fourier decomposition of $\Delta P(\xi)$ is given in Appendix A.

Four boundary conditions are required to specify the dynamical problem. In accordance with the above setup, we impose

$$\xi(x_1=0)=\varepsilon_h\Phi(t),\quad\left(\frac{\partial\xi}{\partial x_1}\right)_{x_1=0}=\varepsilon_p\Psi(t),\quad\left(\frac{\partial^2\xi}{\partial x_1^2}\right)_{x_1=1}=\left(\frac{\partial^3\xi}{\partial x_1^3}\right)_{x_1=1}=0, \tag{3}$$

requiring that the plate displacement and slope at $x_1=0$ follow the leading edge actuation, and that the trailing edge is moment- and force-free.

The problem is analyzed by taking the Fourier transform of Eqs. (1) and (3). Defining the Fourier transform of a function

$$\overline{g}(\omega)=\int_{-\infty}^{\infty}g(t)\mathrm{e}^{-\mathrm{i}\omega t}\,\mathrm{d}t \tag{4}$$

and applying to (1) and (3), yield

$$-\mu\omega^2\overline{\xi}+\frac{\mu}{\alpha^2}\overline{\xi}''''-\Delta\overline{P}(\overline{\xi})=0, \tag{5}$$

together with

$$\overline{\xi}(0)=\varepsilon_h\overline{\Phi}(\omega),\quad\overline{\xi}'(0)=\varepsilon_p\overline{\Psi}(\omega),\quad\overline{\xi}''(1)=\overline{\xi}'''(1)=0, \tag{6}$$

where primes denote differentiations with x_1.

For later convenience, the problem for $\overline{\xi}$, consisting of a homogeneous equation and non-homogeneous boundary conditions, is transformed into a non-homogeneous equation with homogeneous boundary conditions. Toward this end, decompose $\overline{\xi}$ into

$$\overline{\xi}(x_1,\omega)=\overline{F}(x_1,\omega)+\varepsilon_h\overline{\Phi}(\omega)+\varepsilon_p x_1\overline{\Psi}(\omega), \tag{7}$$

and substitute to (5)–(6). This yields an equation for $\overline{F}$

$$-\mu\omega^2\overline{F}+\frac{\mu}{\alpha^2}\overline{F}''''-\Delta\overline{P}(\overline{F})=\overline{\mathcal{F}}_e(x_1,\omega), \tag{8}$$

in conjunction with the boundary conditions

$$\overline{F}(0)=\overline{F}'(0)=\overline{F}''(1)=\overline{F}'''(1)=0. \tag{9}$$

The forcing term appearing on the RHS of Eq. (8) is

$$\overline{\mathcal{F}}_e(x_1,\omega)=\mu\omega^2[\varepsilon_h\overline{\Phi}(\omega)+\varepsilon_p x_1\overline{\Psi}(\omega)]+[\varepsilon_h\overline{\Phi}(\omega)\Delta\overline{P}(1)+\varepsilon_p\overline{\Psi}(\omega)\Delta\overline{P}(x_1)]. \tag{10}$$

The solution for $\overline{F}(x_1,\omega)$ is calculated numerically for prescribed leading edge actuation ($\overline{\Phi}$ and $\overline{\Psi}$) and ω, using the Chebyshev collocation method [46]. The actual plate deflection is obtained by substituting $\overline{F}(x_1,\omega)$ into (7), and taking the

inverse Fourier transform of the result

$$\xi(x_1,t)=\frac{1}{2\pi}\int_{-\infty}^{\infty}\overline{\xi}(x_1,\omega)\mathrm{e}^{\mathrm{i}\omega t}\,\mathrm{d}\omega. \tag{11}$$

3. Acoustic radiation

The far-field acoustic pressure is governed by the nondimensional inhomogeneous wave equation [3,47]

$$\left(M^2\frac{\partial^2}{\partial t^2}-\nabla^2\right)p=\frac{\partial v_\perp}{\partial t}\delta(x_2)+\nabla\cdot\left(\boldsymbol{\gamma_w}\times\hat{\mathbf{U}}\right), \tag{12}$$

where $M=U/c_0\ll 1$ is the mean-stream Mach number, c_0 is the speed of sound, and δ is the Dirac delta function. The two terms on the RHS of Eq. (12) describe the sources of sound. The first term represents the contribution of direct plate motion, where $v_\perp(x_1,\tau)$ is the normal plate velocity oriented into the fluid

$$v_\perp(x_1,t)=\pm\frac{\partial\xi}{\partial t}\quad\text{on}\quad x_2=\pm 0, \tag{13}$$

and the second term represents the contribution of trailing edge vorticity, where $\hat{\mathbf{U}}=\hat{\mathbf{i}}_\mathbf{1}$ is a unit vector in the direction of the mean flow velocity and $\boldsymbol{\gamma_w}$ denotes the vorticity distribution along the trailing edge wake (see (A1)). The Fourier transform of the latter is specified by the Kutta condition [45]

$$\overline{\boldsymbol{\gamma}}_w=\hat{\mathbf{i}}_\mathbf{3}\delta(x_2)\gamma_{w_0}(\omega)\mathrm{e}^{-\mathrm{i}\omega x_1}, \tag{14}$$

where

$$\gamma_{w_0}(\omega)=-\frac{8\int_0^1\sqrt{\frac{s}{1-s}}[\mathrm{i}\omega\overline{\xi}(s,\omega)+\overline{\xi}'(s,\omega)]\,\mathrm{d}s}{\pi[H_1^{(2)}(\omega/2)+\mathrm{i}H_0^{(2)}(\omega/2)]} \tag{15}$$

and $H_n^{(m)}$ denotes the Hankel function of mth kind and nth order.

In accordance with the form of the linearized acoustic equation (12), the acoustic pressure can be written as a sum of "plate motion" and "wake-induced" pressure contributions

$$p(\mathbf{x},t)=p_\xi(\mathbf{x},t)+p_w(\mathbf{x},t), \tag{16}$$

where

$$p_\xi(\mathbf{x},t)=\frac{\partial}{\partial t}\int_{-\infty}^{\infty}\oint_{S_p}v_\perp(\mathbf{y},\tau)G_a(\mathbf{x},\mathbf{y},t-\tau)\,\mathrm{d}S(\mathbf{y})\,\mathrm{d}\tau \tag{17}$$

and

$$p_w(\mathbf{x},t)=-\int_{-\infty}^{\infty}\int_{V_w}(\boldsymbol{\gamma}_w\times\hat{\mathbf{U}})\cdot\nabla G_a(\mathbf{x},\mathbf{y},t-\tau)\,\mathrm{d}^3\mathbf{y}\,\mathrm{d}\tau. \tag{18}$$

In (17)–(18), S_p is the plate surface, V_w denotes the fluid region occupied by the trailing edge wake, and $G_a(\mathbf{x},\mathbf{y},t-\tau)$ is the acoustic Green's function having a vanishing normal derivative on the undisturbed plate.

In the following we assume that the plate is acoustically compact, i.e. that $L/\lambda_k\ll 1$, where $\lambda=2\pi/k$ is the dimensional acoustic wavelength, and $k=\omega U/Lc_0$ is the dimensional acoustic wavenumber. The condition for plate compactness is therefore that $L/\lambda_k=M\omega/2\pi\ll 1$, in accordance with the low Mach assumption set in (12).[1] The compact approximation of the Green's function [3,47]

$$G_a(\mathbf{x},\mathbf{y},t-\tau)=\frac{1}{4\pi|\mathbf{X}-\mathbf{Y}|}\delta(t-\tau-M|\mathbf{X}-\mathbf{Y}|) \tag{19}$$

is applied to evaluate the far-field acoustic radiation. Here $\mathbf{X}(\mathbf{x})$ and $\mathbf{Y}(\mathbf{y})$ are the Kirchhoff vectors for the plate. We approximate $\mathbf{Y}(\mathbf{y})$ by the Kirchhoff vector for a strip

$$\mathbf{Y}(\mathbf{y})=\left(y_1,\mathrm{Re}\left[-\mathrm{i}\sqrt{\left(y_1-\frac{1}{2}+\mathrm{i}y_2\right)^2-\frac{1}{4}}\right],y_3\right), \tag{20}$$

and focus on the far-field ($|\mathbf{X}|\sim|\mathbf{x}|\to\infty$) radiation to approximate the above $G_a(\mathbf{x},\mathbf{y},t-\tau)$ by

$$G_a(\mathbf{x},\mathbf{y},t-\tau)\approx\frac{1}{4\pi|\mathbf{x}|}\delta(t-\tau-M|\mathbf{x}|)+M\frac{\mathbf{x}\cdot\mathbf{Y}}{4\pi|\mathbf{x}|^2}\frac{\partial}{\partial t}[\delta(t-\tau-M|\mathbf{x}|)],\quad|\mathbf{x}|\to\infty. \tag{21}$$

[1] Compactness is assured by considering actuations with $\omega\lesssim O(1)$ (see Section 4). In cases where the actuation signal contains large frequencies, it will be demonstrated that their contribution to the acoustic field is negligible, thus the compact condition is satisfied (see Section 5).

To evaluate $p_{\bar{\xi}}(\mathbf{x},t)$, substitute (21) into (17) and specify the path of integration to obtain

$$p_{\bar{\xi}}(\mathbf{x},[t]) \approx \frac{Mlx_2}{2\pi L|\mathbf{x}|^2}\frac{\partial^2}{\partial t^2}\int_0^1 v_\perp(y_1,[t])\sqrt{y_1(1-y_1)}\,dy_1, \tag{22}$$

where $[t]=t-M|\mathbf{x}|$ is the *acoustic retarded time*. Substitute (13) together with (11) and the definition $x_2=|\mathbf{x}|\cos\theta$ (with $0\le\theta\le\pi$ indicating the observer direction) into (22), to yield

$$p_{\bar{\xi}}(|\mathbf{x}|,\theta,[t]) \approx -\frac{iMl\cos\theta}{4\pi^2 L|\mathbf{x}|}\int_{-\infty}^{\infty}\omega^3 e^{i\omega[t]}\int_0^1 \overline{\xi}(y_1,\omega)\sqrt{y_1(1-y_1)}\,dy_1 d\omega. \tag{23}$$

To calculate $p_w(\mathbf{x},t)$, substitute (14) into (18) and expand for $|\mathbf{x}|\to\infty$. Following a procedure similar to that carried out for $p_{\bar{\xi}}(\mathbf{x},t)$, obtain

$$p_w(|\mathbf{x}|,\theta,[t]) \approx -\frac{iMl\cos\theta}{4\pi^2 L|\mathbf{x}|}\int_{-\infty}^{\infty}\omega\gamma_{w_0}(\omega)e^{i\omega[t]}\int_1^\infty \left(\frac{\partial Y_2}{\partial y_2}\right)_{y_2=0} e^{-i\omega y_1}\,dy_1\,d\omega, \tag{24}$$

where $\gamma_{w_0}(\omega)$ is given by (15). Making use of (20), the y_1-integration in (24) can be carried out explicitly to yield

$$\int_1^\infty \left(\frac{\partial Y_2}{\partial y_2}\right)_{y_2=0} e^{-i\omega y_1}dy_1 = -\frac{\pi}{2}e^{-i\omega/2}H_1^{(1)}(-\omega/2). \tag{25}$$

Substitute (25) and (15) into (24) to obtain

$$\begin{aligned} p_w(|\mathbf{x}|,\theta,[t]) \approx -\frac{iMl\cos\theta}{\pi^2 L|\mathbf{x}|}\int_{-\infty}^{\infty}&\frac{\omega e^{[i\omega([t]-1/2)]}H_1^{(1)}(-\omega/2)}{H_1^{(2)}(\omega/2)+iH_0^{(2)}(\omega/2)} \\ &\times\int_0^1\sqrt{\frac{s}{1-s}}[i\omega\overline{\xi}(s,\omega)+\overline{\xi}'(s,\omega)]\,ds\,d\omega. \end{aligned} \tag{26}$$

The total far-field acoustic pressure is therefore given by the sum of (23) and (26),

$$p(|\mathbf{x}|,\theta,[t]) \approx -\frac{Ml\cos\theta}{4\pi^2 L|\mathbf{x}|}[\Pi_{\bar{\xi}}([t])+\Pi_w([t])], \tag{27}$$

where $\Pi_{\bar{\xi}}([t])$ and $\Pi_w([t])$ are obtained from expressions (23) and (26), respectively, scaled by the common factor multiplying the square brackets in (27).

For later reference, it is instructive to decompose the acoustic pressure into "rigid body" and "elastic motion" components. This is achieved by separating $\overline{\xi}$ in (7) into

$$\overline{\xi}_{\text{rigid}} = \varepsilon_h\overline{\Phi}(\omega)+\varepsilon_p x_1\overline{\Psi}(\omega) \quad\text{and}\quad \overline{\xi}_{\text{elastic}} = \overline{F}(x_1,\omega). \tag{28}$$

Consequently, the total acoustic pressure can be written in the form

$$p(|\mathbf{x}|,\theta,[t]) \approx -\frac{Ml\cos\theta}{4\pi^2 L|\mathbf{x}|}[\Pi_{\text{rigid}}([t])+\Pi_{\text{elastic}}([t])], \tag{29}$$

where $\Pi_{\text{rigid}}([t])$ and $\Pi_{\text{elastic}}([t])$ are obtained by substituting the respective "rigid" and "elastic" components in (28) into $\overline{\xi}$ in (23) and (26).

4. Periodic actuation

Consider the system response to sinusoidal actuation, where leading edge displacement and rotation are applied at a common frequency Ω. The transformed boundary conditions (6) at $x_1=0$ are

$$\overline{\xi}(0) = 2\pi\varepsilon_h\delta(\omega-\Omega) \quad\text{and}\quad \overline{\xi}'(0) = 2\pi\varepsilon_p\delta(\omega-\Omega)e^{i\varphi}, \tag{30}$$

where $0\le\varphi<2\pi$ denotes a phase shift between pitching and heaving. The numerical solution is obtained by substituting

$$\overline{\xi}(x_1,\omega) = 2\pi\delta(\omega-\Omega)[\overline{F}_0(x_1,\omega)+\varepsilon_h+\varepsilon_p e^{i\varphi}x_1] \tag{31}$$

into (5) (cf. (7)), dividing through by the delta-function, and solving for $\overline{F}_0(x_1,\omega)$. The inverse Fourier transform (11) of (31) then results in replacing ω with Ω in the time-domain solution.

4.1. Dynamical response

Fig. 2 presents a typical result for the system response to sinusoidal actuation. In general, it is expected that the frequency spectrum of the forced motion would reflect the unforced (homogeneous) properties of the system, governed by μ and α. The unforced linearized stability problem has been studied previously [21–25,27,43], and a summary of the results is presented in Appendix B and Fig. 10. Our objective is to study the motion of the body forced by leading edge

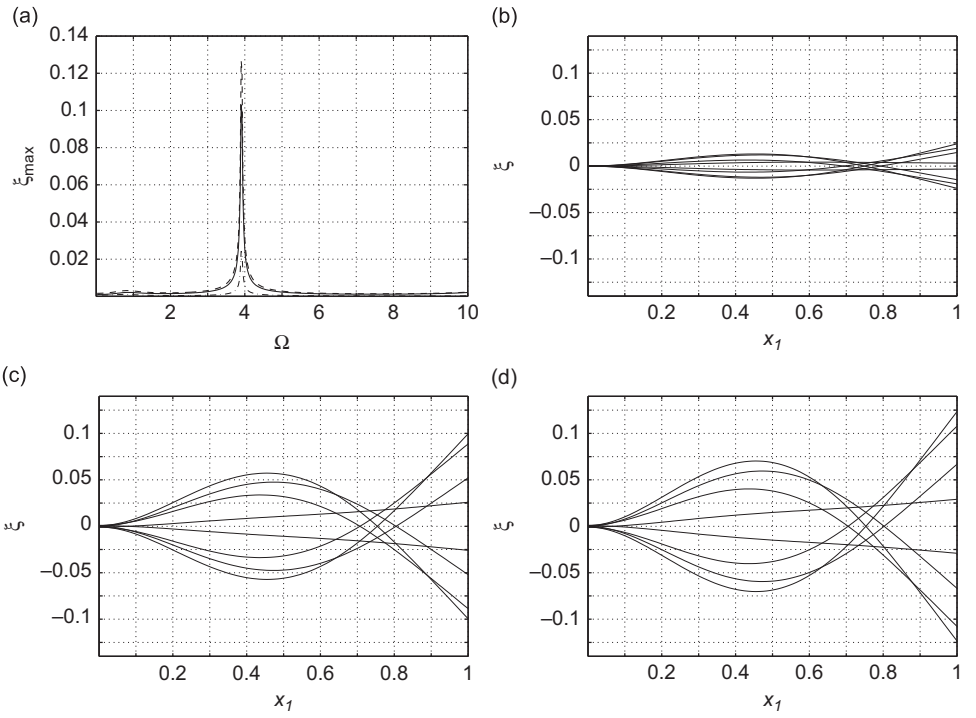

Fig. 2. (a) Frequency spectrum of maximum trailing edge displacement and (b)–(d) time-variation of plate shape for a sinusoidally actuated plate with $\mu=4.5$ and $\alpha=5$. The curves in Fig. 2a correspond to actuations of heaving with no pitching ($\varepsilon_h=10^{-3}$ and $\varepsilon_p=0$, solid line), pitching with no heaving ($\varepsilon_h=0$ and $\varepsilon_p=10^{-3}$, dash-dotted line) and in-phase pitching with heaving ($\varepsilon_h=\varepsilon_p=10^{-3}$ and $\varphi=0$, dashed line). In (b)–(d), the envelopes of motion at the resonance frequency $\Omega_{res}\approx 3.9$ are shown at the same $\varepsilon_p,\varepsilon_h$ and φ combinations: $\varepsilon_h=10^{-3},\varepsilon_p=0$ (b); $\varepsilon_h=0,\varepsilon_p=10^{-3}$ (c); and $\varepsilon_h=\varepsilon_p=10^{-3},\varphi=0$ (d).

actuation. We therefore focus on conditions where the unforced flat plate is stable to small perturbations. We consider a parameter combination typical for insect wings in air [15,17,43] and take $\rho_s\approx 1100\ \mathrm{kg/m^3}$, $\lambda/L\approx 5\times 10^{-3}$, $E\approx 100\ \mathrm{MPa}$, $\nu\approx 0.3$ and $\rho_0\approx 1.2\ \mathrm{kg/m^3}$. Substituting these into μ and α in (2) yield $\mu\approx 4.5$ and $\alpha\approx U/0.45$, where U is measured in SI units. According to the neutral curve presented in Fig. 10 (see Appendix B), the critical value of α for the onset of plate motion at $\mu=4.5$ is $\alpha_c\approx 6.5$. Consequently, our present discussion is confined to $\alpha\lesssim 6.5$. In reference to the above value of $U_b\approx 0.45\ \mathrm{m/s}$, this upper bound on α corresponds to a wind speed of $U\lesssim 3\ \mathrm{m/s}$, consistent with the low-Mach assumption set for the evaluation of the far-field acoustic pressure in Section 3.

Taking $\mu=4.5$ and $\alpha=5$, Fig. 2 presents the frequency response of the plate to sinusoidal actuation at three combinations of $\varepsilon_h,\varepsilon_p$ and φ. The coupling between the forced response and unforced plate properties is manifested through a resonance occurring at the plate least stable eigenfrequency. This is observed in Fig. 2a, where sharp peaks in the maximal trailing edge deflection are obtained at $\Omega=\Omega_{res}\approx 3.9$. The occurrence of the resonance at the same frequency for different combinations of $\varepsilon_p,\varepsilon_h$ and φ is expected, since it is only the combination of μ and α that determines the value of resonance frequency. Yet, the magnitude of the resonance peak is governed by ε_p and ε_h: when both heaving and pitching actuations are applied with no phase shift, this magnitude is maximal [see the dashed line in Fig. 2(a)]. In Fig. 2(b)–(d), the corresponding motion envelopes for the wing are presented at the resonance frequency $\Omega_{res}\approx 3.9$. Note the large ratio between trailing edge ($\sim O(10^{-1})$) and leading edge ($\sim O(10^{-3})$) deflections, resulting from increased energy transfer from the leading edge driver to the free end at resonance conditions. Again we observe that the general form of motion envelope is similar between Fig. 2(b)–(d) (with only the amplitude varying), since it originates from the excitation of the same least stable eigenmode of the unforced system.

A phenomenon similar to the resonance detected in Fig. 2 was found in Ref. [43] for the motion induced in an elastic sheet by a line vortex convected above it. Yet, the two problems are qualitatively different: while in the present setup the external actuation is characterized by a single (prescribed) frequency, the convected vortex in Ref. [43] contains the entire spectrum of frequencies, enabling the system to "pick" the resonance frequency and amplify it. In addition, the nature of resonance in the two cases is different: in the present case the energy is supplied to the system continuously, leading to a non-decaying motion; however, in the vortex-induced problem, the structure motion decays after the passage of the vortex owing to the negative growth rate of the excited eigenmode. In this respect, the present linear-theory results should be taken with some caution: strictly, when actuating the system at the exact eigenmode frequency, the continuous supply of energy may result in considerably large deflections. However, as long as the actuation amplitudes ε_p and ε_h are small enough and the decay rate of the excited eigenmode is large enough, the linearized scheme should suffice to describe the

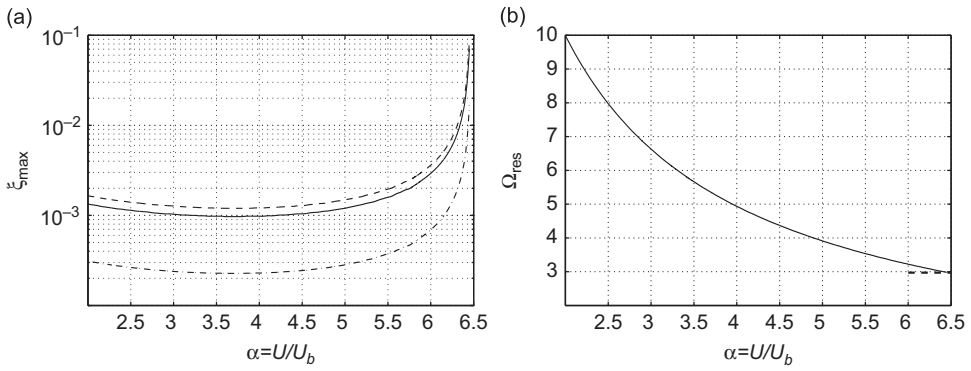

Fig. 3. Effect of normalized wind speed $\alpha = U/U_b$ on maximum trailing edge displacement and resonance frequency for a sinusoidally actuated plate with $\mu = 4.5$. (a) Maximum displacements for $\varepsilon_h = 10^{-5}, \varepsilon_p = 0$ (solid line); $\varepsilon_p = 10^{-5}, \varepsilon_h = 0$ (dash-dotted line); $\varepsilon_p = \varepsilon_h = 10^{-5}$ and $\varphi = 0$ (dashed line). (b) The variation of resonance frequency, corresponding to the three curves presented in (a). The three curves in (b) collapse on the same solid line, which marks the α-variation of the least stable eigenfrequency of the unforced system at $\mu = 4.5$. The bold dashed line marks the critical frequency $\Omega \approx 2.97$ characterizing the onset of unforced plate motion at $\alpha_c \approx 6.5$.

system behavior in the vicinity of Ω_{res}. Indeed, in all the results presented, the condition $\xi_{\max} \ll 1$ is satisfied (see Figs. 2–4 and 6–8).

Fig. 3 describes the effect of normalized wind speed α on the maximum trailing edge displacement (Fig. 3(a)) and resonance frequency (Fig. 3(b)) at $\mu = 4.5$ and three combinations of ε_p, ε_h and φ. At low values of the normalized wind speed ($\alpha \lesssim 5.5$) we note that the motion amplitude is slightly non-monotonic with α and a mild minimum is observed at $\alpha \approx 4$. However, this effect is minor (notice the logarithmic scale of the y-axis) relative to the large increase in amplitude occurring for $\alpha \gtrsim 5.5$: as the relative wind speed approaches its critical value ($\alpha_c \approx 6.5$ for the present value of $\mu = 4.5$; see Fig. 10), the effect of resonance becomes considerably more pronounced. Similarly to the results of Fig. 2, we find that the no-heaving ($\varepsilon_h = 0$) case excites the lowest amplitudes of motion and that the combination of in-phase pitching and heaving results in the largest deflections. Traversing to Fig. 3(b), we note that the resonance frequency, which is equal to the least stable eigenfrequency of the unforced problem, decreases with increasing α. As α approaches its critical $\alpha_c \approx 6.5$ value, the frequency tends to its critical value at the onset of plate motion, $\Omega \approx 2.97$, marked by the bold dashed line in Fig. 3(b) (cf. Fig. 2(b) in [43]). The location of resonance frequencies in Fig. 3(b) is found identical for all combinations of ε_p, ε_h and φ presented in Fig. 3(a).

4.2. Acoustic field

To study the effect of plate elasticity on sound radiation, Fig. 4 compares between the acoustic radiations of elastic and rigid plates. Fig. 4(a) presents the variation of the acoustic pressure amplitude with the actuation frequency Ω, for rigid [Π_{rigid} in (29)] and elastic [the total $\Pi = \Pi_{\mathrm{rigid}} + \Pi_{\mathrm{elastic}}$ in (29)] plates. The rigid and elastic plates are actuated at the same in-phase pitching and heaving conditions. The effect of plate elasticity on sound radiation is observed: while the acoustic pressure amplitude of a rigid plate increases monotonically with Ω, the acoustic pressure radiated in the elastic case exhibits a sharp maximum at $\Omega = \Omega_{\mathrm{res}} \approx 3.9$. This maximum originates from the resonance motion described in Fig. 2(a), so that in the vicinity of $\Omega = \Omega_{\mathrm{res}}$ the sound level emitted by an elastic plate is considerably larger than that of a rigid plate. However, at frequencies far from Ω_{res}, the situation changes qualitatively and the acoustic pressure generated by the elastic plate drops considerably. Specifically, for $\Omega \gtrsim 5.2$ the sound level of the elastic plate becomes lower than the rigid plate, indicating that at frequencies far from Ω_{res} a rigid plate is noisier than an elastic plate. This suggests that at these frequencies plate elasticity acts as an "energy absorber", causing a reduction in the emitted sound level.

To rationalize the above result, Fig. 4(b)–(d) shows the total trailing edge displacements along one period together with their rigid (ξ_{rigid}) and elastic ($\xi_{elastic}$) components [see (28)] for $\Omega = 3.9, 5.2$ and 8. Fig. 4(b) presents the displacements at the resonance frequency $\Omega_{\mathrm{res}} \approx 3.9$: here the plate motion is dominated entirely by the elastic contribution (the dash-dotted line almost coincides with the solid line), leading to noise levels significantly higher than in the rigid plate setup. However, at $\Omega = 5.2$ [Fig. 4(c)] the situation changes qualitatively: the magnitudes of rigid- and elastic-motion components become similar, resulting in comparable noise levels. At higher frequencies [$\Omega = 8$, Fig. 4(d)], the elastic motion component tends to reduce the rigid motion component [acting approximately at opposite phase; cf. the dash-dotted and dashed curves in Fig. 4(d)]. As a result, the total deflection of an elastic plate in this case [solid line in Fig. 4(d)] is smaller than a rigid plate, and the noise level is reduced.

To analyze the separate effects of "plate motion" noise and trailing edge noise on the total acoustic pressure, Fig. 5 presents the frequency dependence of the normalized acoustic pressure amplitude $\Pi = \Pi_\xi + \Pi_w$ together with plate-motion (Π_ξ) and trailing edge noise (Π_w) components [see (27)] for $\mu = 4.5$, $\alpha = 5$, $\varepsilon_p = \varepsilon_h = 10^{-3}$ and $\varphi = 0$. All three curves follow the same sharp-peak pattern, resulting from the resonance motion of the plate. Remarkably, the Π_w component

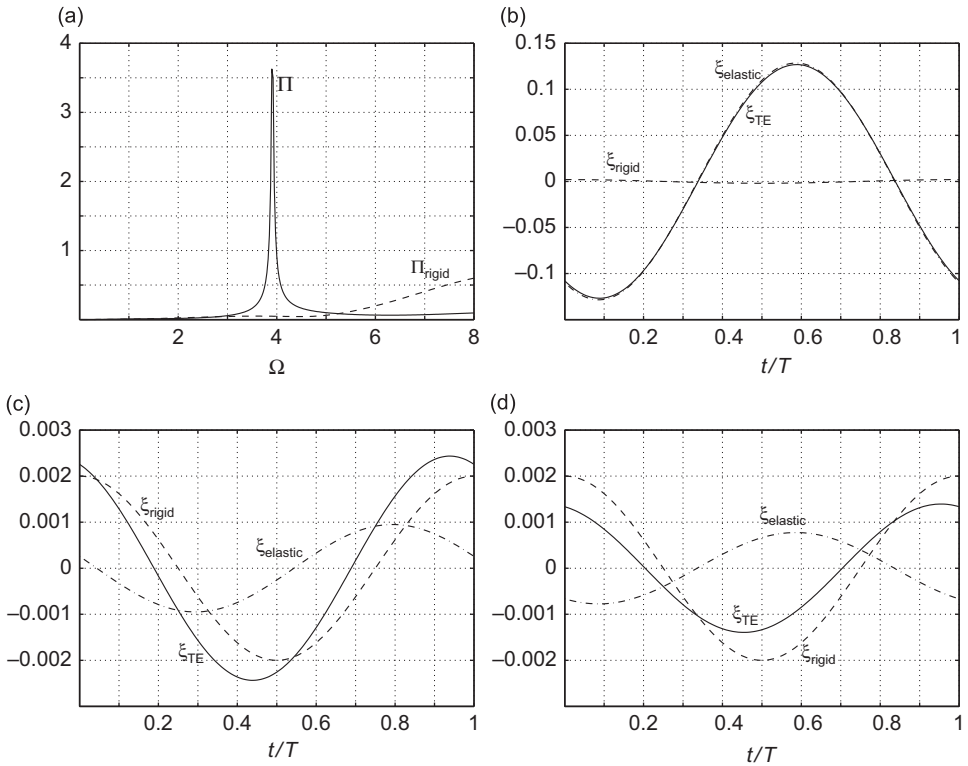

Fig. 4. Effect of plate elasticity on acoustic radiation of a sinusoidally actuated plate with $\mu=4.5$, $\alpha=5$, $\varepsilon_p=\varepsilon_h=10^{-3}$ and $\varphi=0$. (a) Frequency variation of acoustic pressure amplitude ($\Pi=\Pi_{\text{rigid}}+\Pi_{\text{elastic}}$, solid line) and counterpart rigid-plate amplitude (Π_{rigid}, dashed line). (b)–(d) Total trailing edge displacement (ξ, solid lines) and its rigid (ξ_{rigid}, dashed lines) and elastic ($\xi_{elastic}$, dash-dotted lines) components (see (28)) for (b) $\Omega=3.9$, (c) $\Omega=5.2$, and (d) $\Omega=8$. The time is scaled by the period, $T=2\pi/\Omega$.

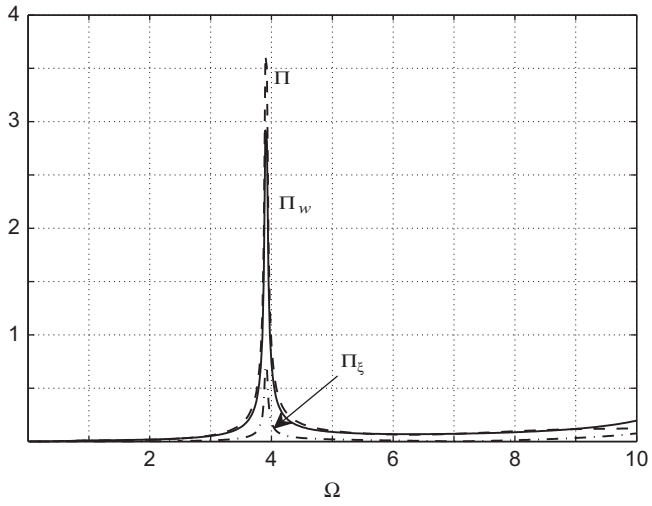

Fig. 5. Frequency dependence of the total pressure amplitude ($\Pi=\Pi_{\text{rigid}}+\Pi_{\text{elastic}}$, dashed line), "plate-motion" acoustic pressure (Π_{ξ}, dash-dotted line), and "wake-induced" pressure (Π_w, solid line), for a sinusoidally actuated plate at $\mu=4.5$, $\alpha=5$, $\varepsilon_p=\varepsilon_h=10^{-3}$ and $\varphi=0$.

contributes most to the total acoustic signal, indicating that the acoustic field is dominated by the effect of trailing edge noise. A similar result was found in Ref. [24], in the context of the sound of an unforced flag. Mathematically, this result is attributed to the square-root singularity of the integrand of γ_{w_0} in (15), which is included in the integral expression for Π_w [see (26) and (27)]. This singularity amplifies the contribution of the trailing edge zone, where deflections are typically the largest [see Fig. 2(b)–(d)], to the integral, compared with the square-root decay of the integrand of Π_{ξ} [see (23) and (27)].

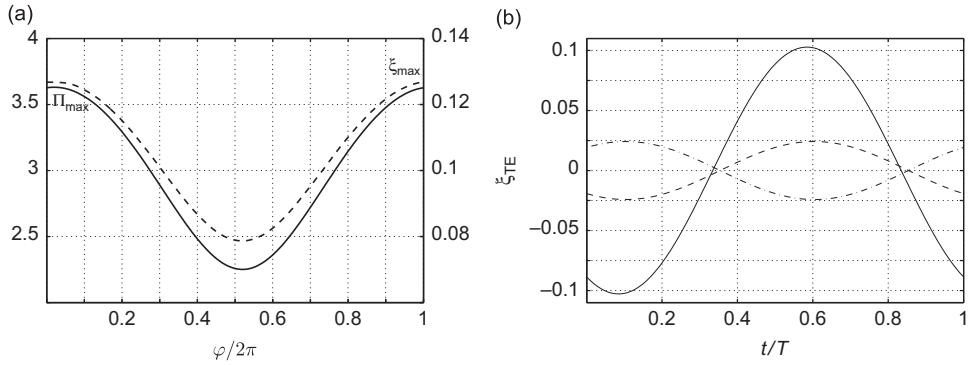

Fig. 6. Effect of phase angle φ on acoustic pressure level and trailing edge displacement for a sinusoidally actuated plate with $\mu=4.5,\alpha=5$. (a) Phase-variation of maximum acoustic pressure Π_{max} ($\Omega=\Omega_{res}\approx 3.9$) at $\varepsilon_p=\varepsilon_h=10^{-3}$ (solid line, left y-axis), and respective maximum trailing edge displacement, ξ_{max} (dashed line, right y-axis). (b) Time-variation of trailing edge displacement ξ_{TE} during a period for $\Omega_{res}\approx 3.9$: $\varepsilon_h=10^{-3},\varepsilon_p=0$ (solid line); $\varepsilon_h=0,\varepsilon_p=10^{-3},\varphi=0$ (dashed line); $\varepsilon_h=0,\varepsilon_p=10^{-3},\varphi=\pi$ (dash-dotted line). The time is scaled by the period, $T=2\pi/\Omega_{res}$.

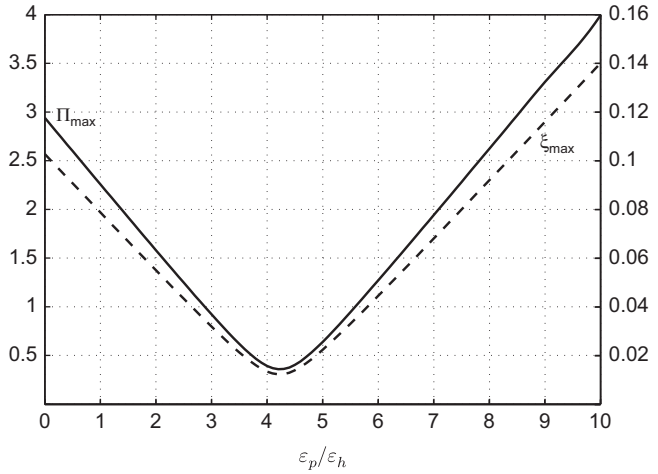

Fig. 7. Effect of $\varepsilon_p/\varepsilon_h$, the ratio between pitching and heaving amplitudes, on acoustic pressure level and amplitude of motion for a sinusoidally actuated plate at $\mu=4.5$, $\alpha=5$, $\varepsilon_h=10^{-3}$ and $\varphi=\pi$. The solid line (left y-axis) presents variation of the maximum acoustic pressure Π_{max} occurring at $\Omega_{res}\approx 3.9$, and the dashed line (right y-axis) shows respective maximum trailing edge displacement.

The effect of phase shift angle φ on the plate motion and acoustic radiation is studied in Fig. 6. The solid line in Fig. 6(a) shows the maximum acoustic pressure (obtained with respect to all frequencies) at $0\le\varphi<2\pi$ for $\mu=4.5$, $\alpha=5$ and $\varepsilon_p=\varepsilon_h=10^{-3}$. The dashed line presents the respective trailing edge amplitude. Both curves follow a symmetrical form with a minimum value at $\varphi\approx\pi$, demonstrating that the plate displacement and sound level are minimized when pitching and heaving are applied at opposite phases. This result is rationalized in Fig. 6(b), which describes the time variation of trailing edge displacement at $\Omega=\Omega_{res}$ and several values of $\varepsilon_h,\varepsilon_p$ and φ. The solid line shows the trailing edge displacement for the case of heaving with no pitching, and the dashed and dash-dotted curves present the cases of pitching with no heaving for $\varphi=0$ and $\varphi=\pi$, respectively. The last two curves are π-shifted from each other, and the corresponding results in Fig. 6(a) can be obtained by taking the maximum value of the sums of the solid and dashed lines (for $\varphi=0$) and the solid and dash-dotted lines (for $\varphi=\pi$). We therefore find that when pitching and heaving are acting in-phase, they amplify the total plate displacement, causing an increase in the acoustic radiation. When acting out of phase, the two signals tend to partially cancel, and this cancelation becomes maximal in the opposite-phase case, $\varphi=\pi$.

To complete the analysis of a sinusoidally actuated plate, Fig. 7 shows the effect of pitching amplitude ε_p, for fixed $\mu=4.5$, $\alpha=5$, $\varepsilon_h=10^{-3}$ and $\varphi=\pi$, on the plate motion and acoustic radiation. According to the results in Fig. 7, both acoustic pressure and trailing edge displacement exhibit a common minimum at $\varepsilon_p\approx 4.2\times 10^{-3}$. This result can be rationalized using Fig. 6(b), by taking the linear superposition of the solid line (showing the trailing edge displacement resulting from heaving actuation only) and the dash-dotted line (showing the displacement resulting from pitching only with $\varphi=\pi$) multiplied by $\varepsilon_p/\varepsilon_h$: when $\varepsilon_p/\varepsilon_h\lesssim 4.2$, the pitching-induced motion acts to reduce the displacement and sound production due to heaving; however, for $\varepsilon_p/\varepsilon_h\gtrsim 4.2$, the contribution of pitching "overcomes" the opposite-phase effect of heaving and becomes dominant. Our calculations indicate that the occurrence of this minimum at some intermediate value of $\varepsilon_p/\varepsilon_h$ takes place in situations where the phase φ between pitching and heaving actuations is nonzero. The value

of $\varepsilon_p/\varepsilon_h$ which minimizes the sound for given $\varphi \neq 0$ varies with φ, and may be a useful mean for controlling the acoustic radiation of the system. The reduction of the acoustic pressure is most efficient in the case $\varphi = \pi$ presented.

5. Non-periodic actuation

The analysis of Sections 2 and 3 is now applied to study the motion and sound generated by non-periodic leading edge actuation. In general, the frequency spectrum of a non-periodic signal includes the entire range of frequencies, $\omega \in (-\infty,\infty)$, and the system response should therefore reflect its resonant behavior by amplifying those frequencies that are closest to the system eigenfrequencies.

To demonstrate this behavior, consider the case of "step-jump" heaving of magnitude ε_h occurring at time $t=0$ in the x_2-coordinate of the leading edge. This can be viewed as a limit case of abrupt change in the plate altitude. Identifying the forms of $\Phi(t)$ and $\Psi(t)$ in (3) with a step-jump actuation, the boundary conditions at the leading edge are

$$\xi(x_1=0)=\varepsilon_h \mathrm{H}(t) \quad \text{and} \quad \left(\frac{\partial \xi}{\partial x_1}\right)_{x_1=0}=0, \tag{32}$$

where $\mathrm{H}(t)$ is a unit step function. The Fourier transform of these conditions yield

$$\overline{\xi}(0)=\varepsilon_h[\pi\delta(\omega)-\mathrm{i}/\omega] \quad \text{and} \quad \overline{\xi}'(0)=0, \tag{33}$$

which determine the general form of the frequency-domain solution

$$\overline{\xi}(x_1,\omega)=\varepsilon_h[\pi\delta(\omega)(\overline{F}_\delta(x_1,\omega)+1)-\mathrm{i}/\omega(\overline{F}(x_1,\omega)+1)]. \tag{34}$$

Taking the inverse Fourier transform (11) of (34), we find that the $\overline{F}_\delta$-term contributes to the time-domain solution only at $\omega=0$. In addition, it can be easily verified that $\overline{F}_\delta(x_1,\omega=0)=0$, as the forcing term (10) vanishes at $\omega=0$. The time-domain solution is therefore

$$\xi(x_1,t)=\frac{\varepsilon_h}{2}\left[2\mathrm{H}(t)-\frac{\mathrm{i}}{\pi}\int_{-\infty}^{\infty}\overline{F}(x_1,\omega)\frac{\mathrm{e}^{\mathrm{i}\omega t}}{\omega}\,\mathrm{d}\omega\right], \tag{35}$$

where $\overline{F}(x_1,\omega)$ is calculated using the scheme of Section 2, and the integral in (35) is evaluated numerically. Although the integral in (35) appears of the form of a principal value integral, it is in practice an ordinary integral since $\overline{F}(x_1,\omega)=0$ at $\omega=0$, similarly to the above $\overline{F}_\delta(x_1,\omega=0)=0$.

Fig. 8 presents the dynamical response and acoustic radiation of a plate actuated by leading edge step-jump with $\varepsilon_h=10^{-2}$, $\mu=4.5$ and $\alpha=5$. Fig. 8(a) shows the trailing edge and mid-point ($x_1=0.5$) displacements, and Fig. 8(b) depicts the total far-field acoustic pressure. At $t<0$, both plate displacement and acoustic radiation vanish. The small-amplitude oscillations observed in the figure result from numerical truncation of the infinite Fourier integral in (35), and it has been verified that extending the limits of numerical integration improves the accuracy of calculation and reduces the error. At $t=0$, the step-jump actuation is applied and initiates sharp variations in plate displacement, accompanied by significant pressure fluctuations. At $0<t\lesssim 3$, the plate trailing edge undergoes considerable "overshoot" deflections between $\xi\approx -0.01$ and $\xi\approx 0.025$, where other parts along the plate follow similar wave-like behavior with reduced amplitudes and varying phases. Coincidentally, relatively high-frequency pressure fluctuations are radiated. This initial transitory behavior of the dynamical system is replaced, at later times ($t\gtrsim 3$), by the appearance of damped oscillations, fluctuating around the new equilibrium state of the plate, $\xi=\varepsilon_h=10^{-3}$. Interestingly, these damped oscillations are dominated by the resonance eigenfrequency of the system, $\Omega_{\mathrm{res}}\approx 3.9$. This confirms the prediction stated in the beginning of the section that the system excitation by an input signal containing the entire frequency spectrum should amplify those frequencies that are closest to the system least stable eigenfrequency. Mathematically, this "frequency amplification" reflects the late-time

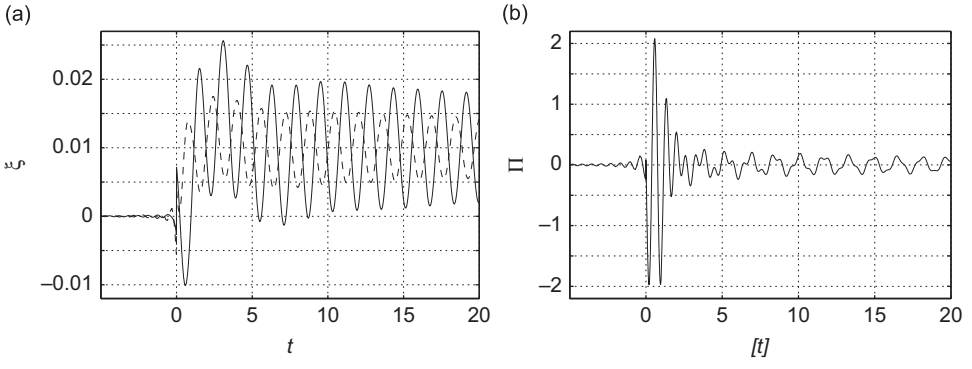

Fig. 8. Motion and acoustic signature of a "step-jump" actuated plate with $\varepsilon_h=10^{-2}$, $\mu=4.5$ and $\alpha=5$. (a) Plate trailing edge (solid line) and mid-point ($x_1=0.5$, dashed line) displacements. (b) Acoustic pressure.

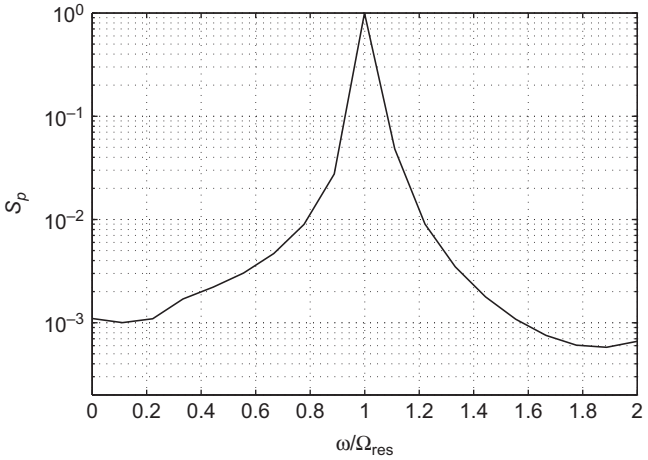

Fig. 9. Power spectrum of the acoustic pressure presented in Fig. 8(b) for $[t] > 5$.

contribution of the poles of the integrand in (35), contained in the explicit form of $\overline{F}(x_1,\omega)$. The most dominant contribution in this case comes from the vicinity of the least stable eigenfrequency, which has the slowest decay rate.

To further analyze the acoustic radiation, Fig. 9 presents the power spectrum $\mathcal{S}_p(\omega)$ of the acoustic pressure presented in Fig. 8(b) for $[t] > 5$. For convenience, the frequency is scaled by Ω_{res} and the power spectrum by $\mathcal{S}_p(\Omega_{\text{res}})$. Following the dynamical behavior of the system, the radiated far-field sound is dominated by the resonance frequency. Unlike in the discrete-spectrum example of Section 4, the continuous spectrum of step-jump actuation radiates sound at frequencies close to Ω_{res} (where the scaled power spectrum is still close to 1). This is reflected by the more "complex" form of the late-time acoustic signature in Fig. 8(b). At later times (not shown here), the plate state converges to its new equilibrium state $\xi = \varepsilon_h$, and the acoustic radiation vanishes.

6. Conclusion

We studied the motion and sound generated by a thin elastic plate subject to uniform low-Mach flow and actuated at its leading edge by arbitrary small-amplitude displacement and rotation. Assuming linearized conditions, a resonance mode of motion was excited in cases where the frequency spectrum of the forcing signal contained an eigenfrequency Ω_{res} of the unforced system. After solving for the plate motion, the dynamical description was used as a "source term" to formulate the acoustic problem. Acoustic radiation of a dipole type was calculated in the limit where the plate is acoustically compact. It was found that plate elasticity can amplify or reduce the sound level (compared to that of a rigid plate), depending on the frequency of external actuation: at frequencies close to Ω_{res}, flexibility results in the generation of increased pressure levels, following the resonance excitation; however, at frequencies far from Ω_{res}, plate elasticity reduces the amplitude of plate deflection (compared to that of a rigid plate), leading to decreased sound levels. In addition, we found that trailing edge noise (resulting from the satisfaction of Kutta condition and subsequent release of trailing edge vorticity) is the main source of sound, dominating the contribution from direct plate motion. When analyzing the acoustic radiation in the case of sinusoidal actuation, the effects of prescribed phase angle φ between pitching and heaving motions, and their amplitudes ε_p and ε_h, were rationalized using the dynamical description. In particular, the existence of specific values of φ and $\varepsilon_p/\varepsilon_h$, where the sound level is minimized, was illustrated.

The results of the present work strongly depend on the assumption of small stream-flow Mach numbers. Thus, the analysis of the source region, consisting of the wing and trailing edge wake, is based on the incompressible theory presented in Refs. [44,45] (see Appendix A). Furthermore, Howe's acoustic analogy (12) used to calculate the far-field sound is based on a small-Mach number assumption ($M^2 \ll 1$), which neglects variations in the speed of sound and propagation of sound by the mean flow. A more thorough analysis is required to study the effect of larger Mach numbers on the present results. Yet, for the purpose of studying the acoustic field generated by typical insect and small-scale flight, the simplifying approximation of small Mach numbers is in place.

A natural extension of the present work would be the consideration of generation of leading edge vorticity on the plate motion and sound. When the plate is actuated at its leading edge, the path of the vortices released there should be influenced by the motion of the plate. However, previous analytical studies (e.g., [30]) have assumed that leading edge vorticity is swept with the mean stream unaffected by the filament motion. Full coupling between the structure motion and leading edge vorticity should therefore be taken into account to study the case where the leading edge is actively displaced. Qualitatively, it is expected that the interaction of leading edge vorticity with an actuated elastic plate would excite a resonance motion even when the actuation frequency does not coincide with one of the system eigenfrequencies, as the incident vorticity itself may consist of a wide range of wavenumbers [43].

The present work extends previous studies of the dynamical problem by considering the system response to arbitrary leading edge actuation and by analysing the far-field acoustic radiation. Apart from the example-cases studied, the analysis can be readily applied to obtain the system response to other small-amplitude (periodic or non-periodic) actuations. Yet, we have focused on conditions where the plate motion is driven entirely by leading edge excitation and all motions of the unforced plate decay. The assumption made on the low amplitudes of applied boundary actuations enabled the use of linear theory and superposition to examine the various effects of trailing edge vorticity and plate elasticity on the acoustic radiation. A desirable extension of the present theory would therefore be to examine the acoustic field at critical and supercritical conditions, where the homogeneous plate response is not trivial, or in cases where the forcing amplitude is large. Such analyzes would require investigation of the non-linear problem, including the interaction between the forced and unforced motion mechanisms. Additional study is also required to incorporate three-dimensional effects, which may have a significant impact on sound radiation in small-scale flapping flight.

Acknowledgment

This work was supported by the Marie Curie International Reintegration Grant no. PIRG-GA-2010-276837.

Appendix A. The fluid loading ΔP

Adopting Theodorsen's linearized analysis of thin-airfoil aerodynamics [44,45], the wing surface and trailing edge wake are represented by thin vortex sheets of vorticities

$$\boldsymbol{\gamma}_{\xi}=\hat{\mathbf{i}}_{\mathbf{3}}\delta(x_2)\gamma_{\xi}(x_1,t) \quad \text{and} \quad \boldsymbol{\gamma}_{\boldsymbol{w}}=\hat{\mathbf{i}}_{\mathbf{3}}\delta(x_2)\gamma_{w}(x_1,t), \tag{A1}$$

corresponding to the wing ($0\le x_1\le 1$) and wake ($1<x_1<\infty$) surfaces, respectively. In (A1), δ denotes the Dirac delta function. Relating the wing vortex sheet to the plate deflection and satisfying the Kutta condition to calculate the strength of trailing edge vorticity, the time Fourier transform of the total pressure jump is obtained

$$\Delta\overline{P}(\overline{\xi})=\frac{4}{\pi}[1-C(\omega/2)]\sqrt{\frac{1-x_1}{x_1}}\int_0^1\sqrt{\frac{s}{1-s}}(\mathrm{i}\omega\overline{\xi}+\overline{\xi}')\,\mathrm{d}s+\frac{2}{\pi}\int_o^1\left[\sqrt{\frac{1-x_1}{x_1}}\sqrt{\frac{s}{1-s}}\frac{1}{x_1-s}-\mathrm{i}\omega\Lambda(x_1,s)\right]\left(\mathrm{i}\omega\overline{\xi}+\overline{\xi}'\right)\mathrm{d}s. \tag{A2}$$

Here

$$\Lambda(x_1,s)=\frac{1}{2}\log\left[\frac{x_1+s-2x_1s+2\sqrt{x_1(1-x_1)}\sqrt{s(1-s)}}{x_1+s-2x_1s-2\sqrt{x_1(1-x_1)}\sqrt{s(1-s)}}\right], \tag{A3}$$

and the function $C(\omega/2)$ is the Theodorsen function [44].

Appendix B. The unforced problem

The eigenvalue problem for the onset of unforced plate motion (Eq. (1) together with the homogeneous counterpart of (3)) has been studied in Ref. [43]. For completeness, Fig. 10 presents the projection of the neutral surface on the (μ,α) plane.

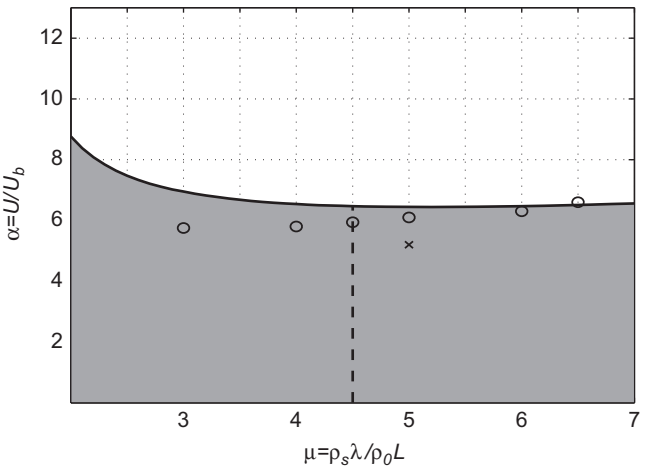

Fig. 10. The neutral curve $\alpha=\alpha_c(\mu)$ for the unforced plate problem, specifying the critical conditions for onset of plate motion. Shaded and unshaded zones mark domains of stability and instability, respectively. The circles and cross denote the theoretical predictions of Kornecki et al. [21] (as presented in Ref. [23]) and Huang [10], respectively. The dashed line ($\mu=4.5, 0<\alpha\lesssim 6.5$) indicates the locus of points considered in Figs. 2–9.

The bold solid line marks the neutral curve, separating between the stable (shaded) and unstable (unshaded) zones. Also presented are the theoretical predictions of Refs. [21] (circles) and [10] (cross) for the neutral curve. The agreement between the results is satisfactory, supporting the application of the present scheme to study of the forced motion and acoustic radiation. While the models used in all the calculations are similar, the quantitative discrepancies between the results may be attributed to the different levels of accuracy applied in the various schemes (see, e.g., the discussion in Section 3.3. of Ref. [21], where the calculation is based on taking only the first two modes in an eigenfunction expansion of the solution).

References

[1] R.D. Blevins, *Flow-Induced Vibration*, Van Nostrand Reinhold, New York, 1990.
[2] M.P. Païdoussis, *Fluid-Structure Interaction: Slender and Axial Flow*, Academic, London, 1998.
[3] M.S. Howe, *Acoustics of Fluid–Structure Interactions*, Cambridge University Press, Cambridge, 1998.
[4] M.J. Shelley, J. Zhang, Flapping and bending bodies interacting with fluid flows, *Annual Review of Fluid Mechanics* 43 (2011) 449–465.
[5] Y. Watanabe, S. Suzuki, M. Sugihara, Y. Sueoka, An experimental study of paper flutter, *Journal of Fluids and Structures* 16 (2002) 529–542.
[6] J.C. Liao, D.N. Beal, G.V. Lauder, M.S. Triantafyllou, Fish exploiting vortices decrease muscle activity, *Science* 302 (2003) 1566–1569.
[7] G.W. Taylor, J.R. Burns, S.M. Kammann, W.B. Powers, T.R. Welsh, The energy harvesting Eel: a small subsurface ocean/river power generator, *IEEE Journal of Oceanic Engineering* 26 (2001) 539–547.
[8] J.J. Allen, A.J. Smits, Energy harvesting Eel, *Journal of Fluids and Structures* 15 (2001) 629–640.
[9] L. Tang, M.P. Païdoussis, J. Jiang, Cantilevered flexible plates in axial flow: energy transfer and the concept of flutter-mill, *Journal of Sound and Vibration* 326 (2009) 263–276.
[10] L. Huang, Flutter of cantilevered plates in axial flow, *Journal of Fluids and Structures* 9 (1995) 127–147.
[11] L. Huang, Mechanical modeling of palatal snoring, *Journal of the Acoustical Society of America* 97 (1995) 3642–3648.
[12] T.M. Grundy, G.P. Keefe, M.V. Lowson, Effects of acoustic disturbances on low Re aerofoil flows, *Progress in Astronautics and Aeronautics* 195 (2001) 91–113.
[13] M. Marcolini, E. Booth, H. Tadghighi, H. Hassan, C. Smith, L. Becker, Control of BVI Noise Using an Active Trailing Edge Flap, Vertical Lift Aircraft Design Conference, San Francisco, CA, 1995.
[14] K. Nguyen, M. Betzina, C. Kitaplioglu, Full-Scale Demonstration of Higher Harmonic Control for Noise and Vibration Reduction on the XV-15 Rotor, *American Helicopter Society 56th Annual Forum*, Virginia Beach, VA, 2000.
[15] T. Maxworthy, The fluid dynamics of insect flight, *Annual Review of Fluid Mechanics* 13 (1981) 329–350.
[16] H.C. Bennet-Clark, Acoustics of insect song, *Nature* 234 (1971) 255–259.
[17] S. Drosopoulos, M.F. Claridge (Eds.), Insect Sounds and Communication: Physiology, Behaviour, Ecology and Evolution, Taylor and Francis, Boca Raton, FL, 2006.
[18] L.J. Cator, B.J. Arthur, L.C. Harrington, R.R. Hoy, Harmonic convergence in the love songs of the dengue vector mosquito, *Science* 323 (2009) 1077–1079.
[19] J. Sueur, E.J. Tuck, D. Robert, Sound radiation around a flying fly, *Journal of the Acoustical Society of America* 118 (2005) 530–538.
[20] Y. Bae, Y.J. Moon, Aerodynamic sound generation of flapping wing, *Journal of the Acoustical Society of America* 124 (2008) 72–81.
[21] A. Kornecki, E.H. Dowell, J. O'Brien, On the aeroelastic instability of two-dimensional panels in uniform incompressible flow, *Journal of Sound and Vibration* 47 (1976) 163–178.
[22] M. Argentina, L. Mahadevan, Fluid-flow-induced flutter of a flag, *Proceedings of the National Academy of Sciences* 102 (2005) 1829–1834.
[23] C. Eloy, R. Lagrange, C. Souilliez, L. Schouveiler, Aeroelastic instability of cantilevered flexible plates in uniform flow, *Journal of Fluid Mechanics* 611 (2008) 97–106.
[24] A. Manela, M.S. Howe, On the stability and sound of an unforced flag, *Journal of Sound and Vibration* 321 (2009) 994–1006.
[25] B.H. Connell, D.K.P. Yue, Flapping dynamics of a flag in a uniform stream, *Journal of Fluid Mechanics* 581 (2007) 33–67.
[26] L. Tang, M.P. Païdoussis, On the instability and the post-critical behaviour of two-dimensional cantilevered flexible plates, *Journal of Sound and Vibration* 305 (2007) 97–115.
[27] S. Alben, M.J. Shelley, Flapping states of a flag in an inviscid fluid: bistability and the transition to chaos, *Physical Review Letters* 101 (2008) 119902.
[28] L. Tang, M.P. Païdoussis, J. Jiang, The dynamics of variants of two-dimensional cantilevered flexible plates in axial flow, *Journal of Sound and Vibration* 323 (2009) 214–231.
[29] V.V. Golubev, B.D. Dreyer, T.M. Hollenshade, M.R. Visbal, High-Accuracy Viscous Analysis of Unsteady Flexible Airfoil Response to Impinging Gust, AIAA Paper No. 2009-3271, 2009.
[30] A. Manela, M.S. Howe, The forced motion of a flag, *Journal of Fluid Mechanics* 635 (2009) 439–454.
[31] R. Godoy-Diana, J.-L. Aider, J.E. Wesfreid, Transitions in the wake of a flapping foil, *Physical Review E* 77 (2008) 016308.
[32] B. Thiria, R. Godoy-Diana, How wing compliance drives the efficiency of self-propelled flapping flyers, *Physical Review E* 82 (2010) 015303.
[33] D. Qi, Y. Liu, W. Shyy, H. Aono, Simulations of dynamics of plunge and pitch of a three-dimensional flexible wing in a low Reynolds number flow, *Physics of Fluids* 22 (2010) 091901.
[34] H. Masoud, A. Alexeev, Resonance of flexible flapping wings at low Reynolds number, *Physical Review E* 81 (2010) 056304.
[35] S. Alben, Optimal flexibility of a flapping appendage in an inviscid fluid, *Journal of Fluid Mechanics* 614 (2008) 355–380.
[36] S. Alben, Simulating the dynamics of flexible bodies and vortex sheets, *Journal of Computational Physics* 228 (2009) 2587–2603.
[37] S. Michelin, S.G. Llewellyn Smith, Resonance and propulsion performance of a heaving flexible wing, *Physics of Fluids* 21 (2009) 071902.
[38] M.S. Howe, The influence of vortex shedding on the generation of sound by convected turbulence, *Journal of Fluid Mechanics* 76 (1976) 711–740.
[39] I.D. Abrahams, Scattering of sound by a heavily loaded finite elastic plate, *Proceedings of the Royal Society of London* 378 (1981) 89–117.
[40] I.D. Abrahams, Scattering of sound by an elastic plate with flow, *Journal of Sound and Vibration* 89 (1983) 213–231.
[41] D.G. Crighton, The 1988 Rayleigh medal lecture: fluid-loading—the interaction between sound and vibration, *Journal of Sound and Vibration* 133 (1989) 1–27.
[42] M.S. Howe, Elastic blade–vortex interaction noise, *Journal of Sound and Vibration* 177 (1994) 325–336.
[43] A. Manela, Sound generated by a vortex convected past an elastic sheet, *Journal of Sound and Vibration* 330 (2011) 416–430.
[44] T. Theodorsen, General Theory of Aerodynamic Instability and the Mechanism of Flutter, NACA Report no. 496 (1935).
[45] R.L. Bisplinghoff, H. Ashley, R.L. Halfman, *Aeroelasticity*, Addison-Wesley, Toronto, 1955.
[46] R. Peyret, *Spectral Methods for Incompressible Viscous Flow*, Springer, New-York, 2002.
[47] M.S. Howe, *Theory of Vortex Sound*, Cambridge University Press, Cambridge, 2003.